^{57}Fe Mössbauer and magnetic studies of $ErFe_{12-x}Nb_x$

2005 J. Phys.: Condens. Matter 17 3689

(http://iopscience.iop.org/0953-8984/17/23/020)

INSTITUTE OF PHYSICS PUBLISHING JOURNAL OF PHYSICS: CONDENSED MATTER

J. Phys.: Condens. Matter **17** (2005) 3689–3700 doi:10.1088/0953-8984/17/23/020

^{57}Fe Mössbauer and magnetic studies of $ErFe_{12-x}Nb_x$

J L Wang[1], S J Campbell[1], J M Cadogan[2], O Tegus[3] and A V J Edge[1]

[1] School of Physical, Environmental and Mathematical Sciences, The University of New South Wales, The Australian Defence Force Academy, Canberra, ACT 2600, Australia
[2] School of Physics, The University of New South Wales, Sydney, NSW 2052, Australia
[3] Van der Waals-Zeeman Institute, University of Amsterdam, 1018 XE Amsterdam, The Netherlands

Received 1 April 2005, in final form 5 May 2005
Published 27 May 2005
Online at stacks.iop.org/JPhysCM/17/3689

Abstract

The structural and magnetic properties of $ErFe_{12-x}Nb_x$ compounds ($x = 0.6$, 0.7 and 0.8) have been investigated by x-ray diffraction, ac susceptibility and dc magnetization measurements and ^{57}Fe Mössbauer spectroscopy. Refinements of the x-ray diffraction patterns show that the Nb atoms preferentially occupy the 8i sites; this can be understood in the terms of enthalpy effects and differences in the metallic radii. The average Fe–Fe distance at the different sites is found to behave as $d_{Fe-Fe}(8i) > d_{Fe-Fe}(8j) > d_{Fe-Fe}(8f)$. The unit cell volume increases slightly with increasing Nb content, consistent with the larger radius of Nb compared with Fe. A spin reorientation from easy-axis at room temperature to easy-cone at low temperatures has been detected for all compounds. The spin reorientation temperatures T_{sr} in $ErFe_{12-x}Nb_x$ compounds remain essentially unchanged ($T_{sr} \sim 42$–44 K) with increasing Nb concentration, whereas a significant decrease in T_{sr} ($T_{sr1} \sim 236$–204 K; $T_{sr2} \sim 154$–94 K) is obtained in $DyFe_{12-x}Nb_x$ from $x = 0.6$ to 0.8. This can be understood by taking the different crystal-field terms responsible for the spin reorientation in the two systems into account. We find that the spin-reorientation process is particularly sensitive to the sixth-order term $B_{60}O_{60}$ of the crystal field acting on the Er^{3+} ion, due to its large and positive value of γ_J. ^{57}Fe hyperfine interaction parameters and magnetic moments values have been determined for the 8i, 8j and 8f sites from the Mössbauer spectra. The weighted average ^{57}Fe hyperfine field values were found to follow a T^2 dependence; this suggests that a single-particle excitation mechanism is responsible for reduction of the 3d-sublattice magnetization with increasing temperature.

(Some figures in this article are in colour only in the electronic version)

1. Introduction

Since the discovery of $Nd_2Fe_{14}B$, rare-earth (R) iron-rich intermetallic compounds with the $ThMn_{12}$-type structure (space group $I4/mmm$, No. 139) have attracted a great deal of attention due to their relatively simple crystal structure and excellent magnetic properties [1]. From a fundamental point of view, the $R(Fe, M)_{12}$ compounds (M = stabilizing element) can provide much useful and critical information related to crystal-field (CEF) and exchange interactions and the interplay between them [2]. However, some inconsistencies exist in the reported magnetic structures and magnetic transitions such as spin reorientation and first-order magnetization transition in $R(Fe, M)_{12}$ compounds [3, 4]. For example, Hu *et al* [2] reported that a first-order spin reorientation takes place at $T_{sr1} = 58$ K in $DyFe_{11}Ti$ (characterized by an abrupt change in the angle θ between the easy magnetization direction and the four-fold axis [001] from $\theta \sim 40°$ to 90°) with a second-order spin reorientation (a continuous change in θ with temperature) at $T_{sr2} = 220$ K, whereas Andreev *et al* [3] reported two consecutive second-order spin reorientations at $T_{sr1} = 120$ and $T_{sr2} = 220$ K.

Such discrepancies in the nature of reported spin reorientation processes or the spin reorientation temperatures can be ascribed to the fact that both the temperature and character of a magnetic phase transition are very sensitive to the external measurement field and the detection methods. Compositional variations may also play a role [3, 4]. Generally, the Curie temperature, T_C, has been found to be sensitive to composition in rare-earth–transition-metal (R–T) compounds and can be regarded as an indicator of differences in composition. In addition, recent investigations of $RFe_{12-x}M_x$ compounds (R = Tb, Dy and M = Ti or Nb) have shown clearly that a slight change in concentration of the stabilizing M element can also lead to a pronounced shift of the spin reorientation temperature even though T_C remains essentially constant [5–7]. Both the Tb^{3+} and Dy^{3+} ions have a negative second-order Stevens coefficient α_J and the CEF lattice coefficient A_{20} in the $R(Fe, M)_{12}$ structure is negative so the second-order CEF favours a basal plane ordering in Fe-rich $R(Fe, M)_{12}$ compounds with R = Tb and Dy. Combining this with the easy-axis Fe-sublattice anisotropy, a spin reorientation in $Tb(Fe, M)_{12}$ and $Dy(Fe, M)_{12}$ can be ascribed to the competition between the R and Fe anisotropies, as a first approximation.

$RFe_{12-x}M_x$ compounds with $R = Er^{3+}$ can exhibit a spin-reorientation transition which is driven mainly by the competition between the different orders of the CEF interactions of the Er^{3+} ion because the Er^{3+} ion has a positive α_J, in contrast to Tb^{3+} and Dy^{3+}. Tetragonal $ThMn_{12}$-type $RFe_{12-x}Nb_x$ compounds with R = Gd, Tb, Dy and Y [5, 7] can only be synthesized in a narrow range of Nb concentration, $x \sim 0.55$–0.9. Here, we investigate $ErFe_{12-x}Nb_x$ with $x = 0.6$–0.8 to clarify the influence of the Nb content on the spin reorientation in these compounds.

2. Experimental details

$ErFe_{12-x}Nb_x$ compounds with $x = 0.6$, 0.7 and 0.8 were prepared by conventional argon arc melting. The samples were characterized by x-ray diffraction (Cu Kα radiation, $\lambda = 1.5418$ Å). The temperature dependence of the ac magnetic susceptibility (frequency range $f = 33$–333 Hz and $H_{rms} = 78$ A m^{-1}) was measured using a variable-temperature helium cryostat and a Lakeshore Cryogenics temperature controller (4.2–300 K). The temperature dependence of the magnetization, $M(T)$, was measured in a magnetic field of $B_{appl} = 0.05$ T in a superconducting quantum interference device (SQUID) from 5 to 300 K. ^{57}Fe Mössbauer spectra were obtained between 4.2 and 298 K using a standard constant-acceleration

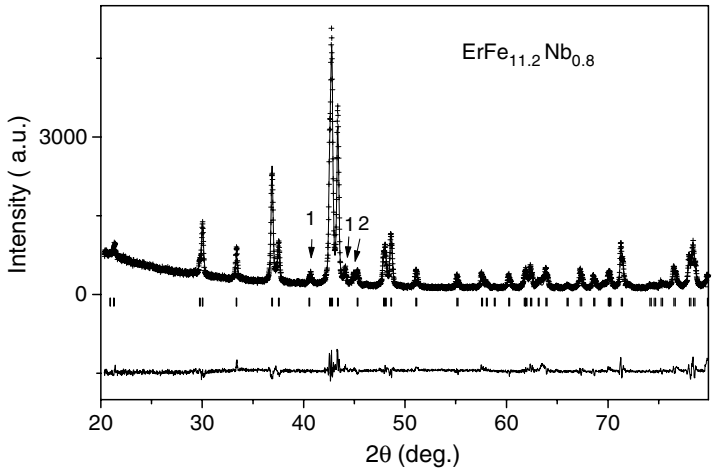

Figure 1. X-ray diffraction pattern (Cu Kα) of $ErFe_{11.2}Nb_{0.8}$ along with the refined and difference patterns. The markers indicate the peak positions for $ErFe_{11.2}Nb_{0.8}$ ($ThMn_{12}$-type structure) with the arrows 1 and 2 indicating the main reflections of the small fractions of Fe_2Nb and α-Fe impurities, respectively (see text).

Table 1. The lattice parameters and atomic positions of $ErFe_{12-x}Nb_x$ ($x = 0.6$, 0.7, 0.8) as determined from Rietveld refinements of the x-ray diffraction patterns (e.g. figure 1 for $ErFe_{11.2}Nb_{0.8}$). The errors for the data in each column were derived from the data fits and are as given for each first entry.

					d_{Fe-Fe} (Å)		
x	a (Å)	c (Å)	x(8i)	x(8j)	8i	8j	8f
0.6	8.488(1) 2.501(1)	4.787(1)	0.360	0.279	2.704(1)	2.574(1)	2.501(1)
0.7	8.497 2.503	4.793	0.358	0.280	2.713	2.577	2.503
0.8	8.499 2.505	4.795	0.359	0.281	2.712	2.578	2.505

spectrometer and a ^{57}CoRh source. The spectrometer was calibrated at room temperature with an α-iron foil.

3. Results and discussion

3.1. Structural behaviour

Analysis of the x-ray diffraction patterns showed that all samples are essentially single phase and have the $ThMn_{12}$-structure as expected, with a total impurity content of less than 4 wt%, α-Fe and Fe_2Nb being the impurity phases. Figure 1 shows the experimental and calculated x-ray diffraction patterns for $ErFe_{11.2}Nb_{0.8}$ as typical examples for the three samples investigated. The pattern factor R_p, the weighted pattern factor R_{wp}, and the expected pattern factor R_{exp} are 7.44, 9.60 and 5.23, respectively. The data were refined by Rietveld analysis using the FULLPROF program [8] and the results of the refinements for all compounds are listed in table 1. According to the Rietveld refinement, the refined values of the Nb content are $x = 0.58$, 0.72 and 0.79, in

good agreement with the nominal values of $x = 0.6, 0.7, 0.8$, respectively. Given the difficulty in determining accurately the small amounts of the impurity phases α-Fe and Fe_2Nb identified in the diffraction patterns, we use the nominal composition in the following analyses. We find that the Nb atoms occupy only the 8i sites in all of the compounds; this can be understood in terms of enthalpy effects and metallic radii. Because Fe–Nb has a more favourable heat of formation of binaries than Er–Nb [9], Nb prefers to occupy the 8i site, which forms only one bond with Er, compared with the 8j and 8f sites, which both have two bonds with Er. Moreover, based on the size effect, the larger Nb atoms also prefer the 8i site, which has the largest Wigner–Seitz cell, compared with the 8j and 8f sites (similar behaviour has been observed in other $RFe_{12-x}M_x$ systems (e.g. M = Ti, Ta, W [10–12], respectively; see also [1])). The unit cell volume is also found to increase slightly with increasing Nb content, consistent with the larger radius of Nb compared with Fe. As shown in table 1, the average Fe–Fe distance at the different Fe/Nb sites varies as follows: $d_{\mathrm{Fe-Fe}}(8i) > d_{\mathrm{Fe-Fe}}(8j) > d_{\mathrm{Fe-Fe}}(8f)$ with the corresponding values increasing slightly with increasing Nb content, x.

3.2. Magnetic behaviour; crystal field analysis

The temperature dependences of the ac susceptibility and the dc magnetization for the $ErFe_{12-x}Nb_x$ compounds are shown in figures 2(a) and (b), respectively. The anomaly ascribed to the spin reorientation from easy-axis at room temperature to easy-cone at low temperature is evident in both the ac and dc measurements in figure 2. In this work we take T_{sr} to be the temperature at which the peak occurs in the ac susceptibility data or the temperature at which the minimum in $\mathrm{d}M/\mathrm{d}T$ occurs in the dc magnetization data. Moreover, we find that the spin reorientation temperatures remain essentially unchanged with increasing Nb content ($T_{\mathrm{sr}} \sim 42$, ~44 and ~44 K for $x = 0.6$, 0.7 and 0.8, respectively). This is in contrast to the cases of $TbFe_{12-x}Nb_x$ ($T_{\mathrm{sr}} \sim$ 406–299 K for $x = 0.6$–0.8) and $DyFe_{12-x}Nb_x$ ($T_{\mathrm{sr1}} \sim$ 236–204 K; $T_{\mathrm{sr2}} \sim$ 154–94 K for $x = 0.6$–0.8) where the spin reorientation temperatures decrease steadily with increasing x. Similar behaviour can also be found in the $RFe_{12-x}V_x$ [13–15] and $RFe_{12-x}Mo_x$ series [16, 17]. In the case of $ErFe_{12-x}V_x$, T_{sr} changes only slightly from ~45 to ~40 K as the V concentration increases from $x = 1.5$ to 2.0, whereas for $DyFe_{12-x}V_x$, T_{sr} varies from ~170 to ~125 K over the x range from 1.5 to 2.75 [13, 15]. Likewise, for $ErFe_{12-x}Mo_x$, when x changes from 1.5 to 2.0, T_{sr} remains relatively unchanged from ~60 to ~65 K, while for $DyFe_{12-x}Mo_x$, T_{sr} varies from ~188 to ~110 K [16, 17] over the same concentration range.

It is widely accepted that the origin of the spin reorientation can be attributed to crystal-field effects. Generally speaking, the origin of a spin reorientation in R–T compounds can be due to either competition between the R and T anisotropies, and/or competition between the second-, fourth- and sixth-order terms of the R^{3+} crystal field. From previous studies [7] it is known that the magnetocrystalline anisotropy of the iron sublattice favours the c-axis. As mentioned earlier, the second-order CEF parameter in $TbFe_{12-x}Nb_x$ and $DyFe_{12-x}Nb_x$ favours the basal plane due to the negative Stevens coefficients α_J of the respective R^{3+} ions, so a spin reorientation can occur in these systems as a result of the competition between the R and T anisotropies. For R = Er, the higher-order CEF parameters should be considered since both the Fe sublattice and the second-order CEF term of Er^{3+} favour the c-axis. The case of the crystal field acting on the Tb^{3+} ion is special due to a suggested admixture of the Tb^{4+} state with the Tb^{3+} state. Attempts to reproduce the magnetic behaviour of $TbFe_{12-x}M_x$ with the same CEF terms as other rare-earths have usually led to disagreement with experimental observations [18, 19]. Here we investigate the behaviour of the $ErFe_{12-x}Nb_x$ and $DyFe_{12-x}Nb_x$ systems in detail.

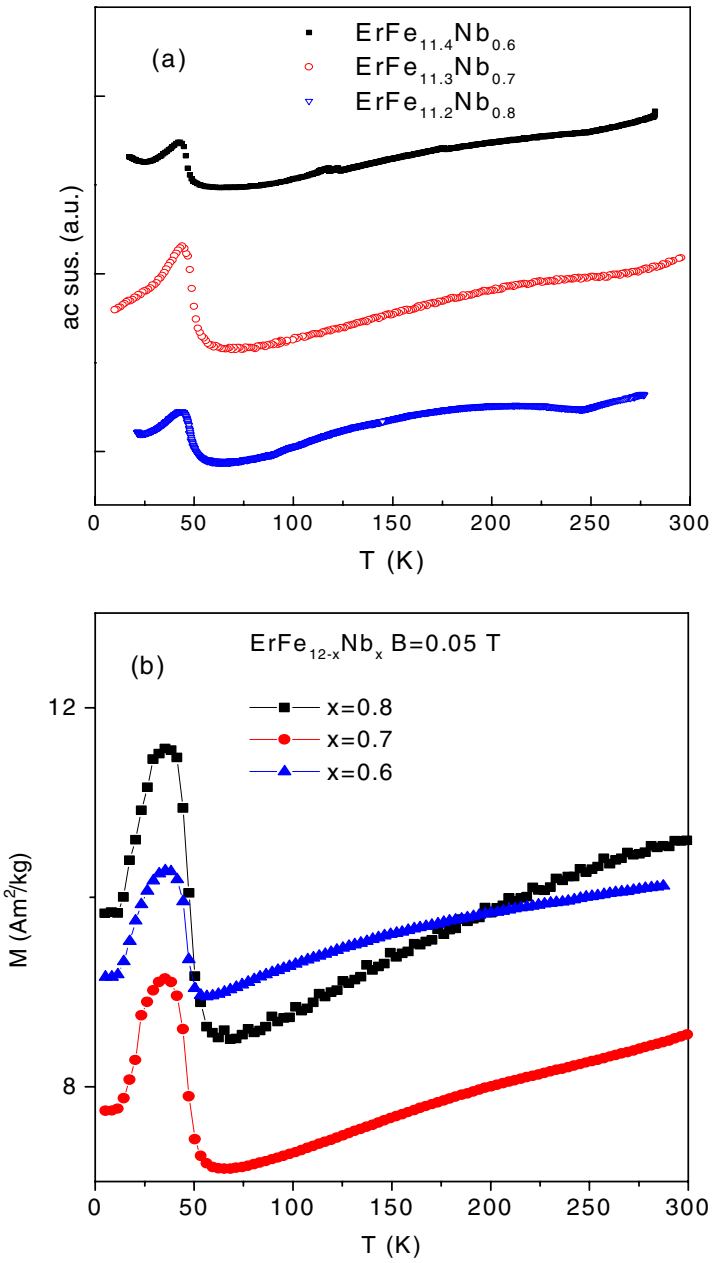

Figure 2. ac and dc magnetic measurements for $ErFe_{12-x}Nb_x$ (4.2–300 K): (a) ac magnetic susceptibility χ ($f = 133$ Hz and $H_{rms} = 78$ A m^{-1}) and (b) dc magnetization ($B_{appl} = 0.05$ T).

Using standard notation, the CEF Hamiltonian at the rare-earth 2a sites in the $ThMn_{12}$-type structure can be written [1, 2, 20, 21]:

$$H_{CEF} = B_{20}O_{20} + B_{40}O_{40} + B_{44}O_{44} + B_{60}O_{60} + B_{64}O_{64}, \quad (1)$$

where the B_{nm} are the CEF parameters and the O_{nm} are the Stevens operator equivalents [1]. For the purpose of classifying the effect of the individual crystal-field coefficients in a

phenomenological way, the anisotropy of the R^{3+} ion in these compounds can be described by the expression:

$$E_R^a = B_{20}\langle O_{20}\rangle[-\tfrac{3}{2}\sin^2\theta] + B_{40}\langle O_{40}\rangle[-5\sin^2\theta + \tfrac{35}{8}\sin^4\theta] + B_{60}\langle O_{60}\rangle[-\tfrac{21}{2}\sin^2\theta + \tfrac{189}{8}\sin^4\theta - \tfrac{231}{16}\sin^6\theta] + B_{44}\langle O_{40}\rangle[\tfrac{1}{8}\cos 4\phi \sin^4\theta] + B_{64}\langle O_{60}\rangle[\tfrac{5}{8}\cos 4\phi \sin^4\theta - \tfrac{11}{16}\cos 4\phi \sin^6\theta], \quad (2)$$

where θ and ϕ are the polar angles of the magnetization vector in a reference frame in which **x** is parallel to [100] and **z** is parallel to [001]. Combined with the Fe sublattice anisotropy, which may be written $E_{Fe}^a = K_1(\mathrm{Fe})\sin^2\theta$, the anisotropy energy for any direction of the total magnetization can be determined, which in turn enables us to clarify the role of each of the CEF parameters. By fitting the temperature dependence of the magnetization of $ErFe_{11.3}Nb_{0.7}$ and $DyFe_{11.3}Nb_{0.7}$ (data derived from [7]), the temperature dependences of M_R have been obtained using molecular-field theory. The temperature dependence of K_1(Fe) was derived from magnetic measurements of the corresponding $YFe_{12-x}Nb_x$ compounds [7], where both K_1(Fe) and M_s gradually decrease with increasing x, while T_C remains almost constant.

We begin our CEF analysis by assuming that the five crystal-field lattice coefficients $\{A_{nm}\}$ are the same as those of a $DyFe_{11}Ti$ single crystal [22] ($A_{20} = -32.3$ K a_0^{-2}, $A_{40} = -12.4$ K a_0^{-4}, $A_{44} = -118$ K a_0^{-4}, $A_{60} = -2.56$ K a_0^{-6}, and $A_{64} = -0.64$ K a_0^{-6}, where a_0 is the Bohr radius. The signs of the CEF coefficients A_{44} and A_{64} have been changed with respect to the values reported in [22], as discussed in [21]). Because the values of $B_{64}\langle O_{60}\rangle$ (-3.61 and -5.75 K for Dy and Er at 0 K, respectively) are much smaller in magnitude than those of $B_{44}\langle O_{40}\rangle$ (172.2 and -109.0 K for R = Dy and Er at 0 K, respectively), the easy magnetization in the (001) plane is actually dominated by the $B_{44}\langle O_{40}\rangle$ and should be along [110], i.e. $\phi = 45°$, for R = Dy and [100], i.e. $\phi = 0°$, for R = Er. So for R = Er, we have canting in the (100) plane whereas for R = Dy the canting takes place within the (110) plane [6, 21, 22]. We have calculated the total anisotropy energy E_a and each of its five components as a function of θ for $ErFe_{12-x}Nb_x$ with $\phi = 0°$ and $DyFe_{12-x}Nb_x$ with $\phi = 45°$ (figures 3 and 4, respectively; the K_1(Fe) data at 5 K are taken from the results for $YFe_{12-x}Nb_x$ [7]). For $ErFe_{11.3}Nb_{0.7}$ it can be seen from the different contributions to E_a (figure 3) that, at 5 K, the easy magnetization direction tends to an intermediate angle of $\theta \sim 25°$. This arises as a result of contributions from the higher-order energy terms, especially, the sixth-order term $B_{60}\langle O_{60}\rangle$ of the CEF, due to the large and positive value of γ_J [20]. In the case of $DyFe_{11.3}Nb_{0.7}$ (figure 4) we see that at low temperatures all the CEF terms except $B_{64}\langle O_{60}\rangle$ contribute to the shift in the easy direction from the c-axis towards the basal plane.

Stefanski and Ivanov [13] attributed the shift of T_{SR} in $DyFe_{12-x}V_x$ to the decrease in the absolute value of A_{20} resulting from the changes in the 8i position and lattice parameters as the V atoms preferentially replace Fe at the 8i sites. This behaviour agrees with our recent investigation of single-crystal $TbFe_{12-x}Ti_x$ [6], where it was concluded from fitting magnetic data with a two-sublattice CEF model that A_{20} shifts towards a more negative value with decreasing x. By estimating the individual CEF terms, Kuz'min [4] reported that the second-order term is the dominant contribution (~85%) to the shift of T_{sr} in $DyFe_{12-x}Ti_x$ compounds ($dT_{sr}/dx \sim -130$ K) and that the shift of A_{20} to positive values plays a critical role in the decrease of T_{sr}. Given the proximity of Nb, Ti, V in the periodic table and the similarity in their chemical properties, similar behaviour for the $RFe_{12-x}Nb_x$, $RFe_{12-x}Ti_x$ and $RFe_{12-x}V_x$ series would not be unexpected. The significant change in T_{sr} in $DyFe_{12-x}Nb_x$ with Nb content can be understood in terms of a large shift of A_{20} resulting from Nb substitution. However, in the case of the $ErFe_{12-x}Nb_x$ system, the spin reorientation is determined by the higher-order CEF terms,

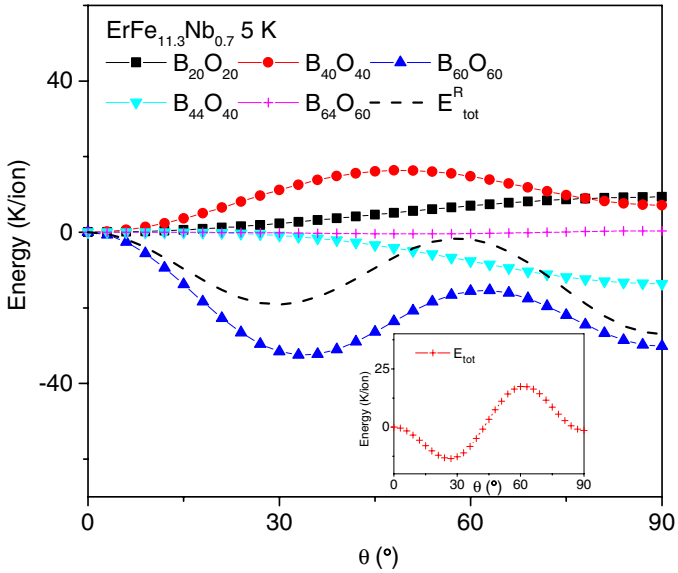

Figure 3. Calculated contributions from the individual CEF terms to the energy surface in the (010) plane of $ErFe_{11.3}Nb_{0.7}$ at 5 K as discussed in the text. The total anisotropy energy is shown in the inset.

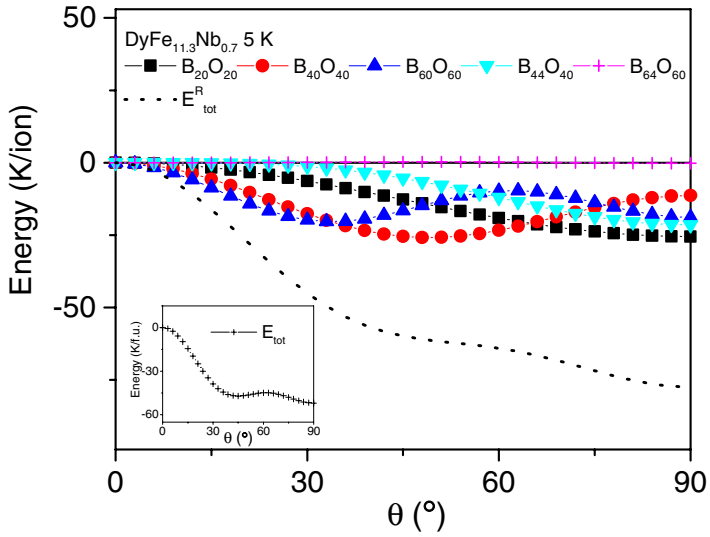

Figure 4. Calculated contributions from the individual CEF terms to the energy surface in the (110) plane of $DyFe_{11.3}Nb_{0.7}$ at 5 K as discussed in the text. The total anisotropy energy is shown in the inset.

and the fact that T_{sr} is essentially invariant with x indicates that the higher-order CEF terms may not be too sensitive to the Nb content, as was suggested for the $ErFe_{12-x}V_x$ system [13]. By using the generalized Brillouin function approach to derive the temperature dependences of the $\langle O_{nm} \rangle$ terms, and taking into account the changes in the crystal-field parameters based on the density functional work of Kuz'min [4], we have calculated the compositional dependence

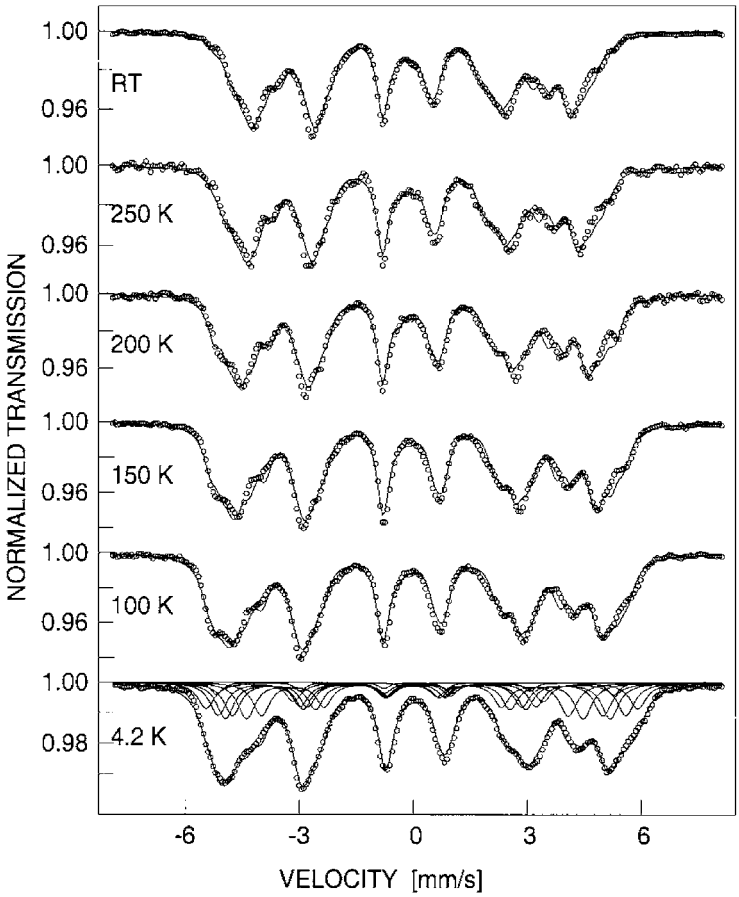

Figure 5. ^{57}Fe Mössbauer spectra of $ErFe_{11.4}Nb_{0.6}$ at various temperatures from 4.2 K to room temperature. The fits to the spectra are described in the text.

of the spin reorientation temperatures for $RFe_{12-x}Nb_x$ with R = Er and Dy ($x = 0.6$–0.8). Our calculations show that the change in T_{sr} is significantly larger for Dy than for Er, in agreement with experimental findings. Details of this work will be published elsewhere [23].

3.3. Mössbauer studies

In figure 5 we show the Mössbauer spectra of $ErFe_{11.4}Nb_{0.6}$ obtained at various temperatures. These spectra are typical of the $ErFe_{12-x}Nb_x$ compounds studied. The iron atoms in $ErFe_{12-x}Nb_x$ occupy three inequivalent 8i, 8j, and 8f crystallographic sites with, as noted above, the Nb atoms occupying only the 8i sites. The spectra were initially analysed using three sextets associated with the 8i, 8j, and 8f sites and with relative areas in the ratios of the site occupancies $(4 - x)$:4:4 of the Fe atoms in $ErFe_{12-x}Nb_x$. The resultant fits provided a general description of the data but failed to accommodate any details. Each sextet was therefore replaced by two sextets in the fitting process in order to approximate the distribution of Nb atoms in the neighbourhood of the three iron sites. Assuming that the Nb atoms occupy the 8i site in a random manner, the iron atoms on the 8f, 8i, and 8j sites would have binomial distributions of near-neighbour Nb environments. In the case of $ErFe_{11.4}Nb_{0.6}$, the 8i sextet is represented

Table 2. Hyperfine fields for the Fe sites and the corresponding Fe magnetic moments (conversion coefficient 15.6 T/μ_B [2]) in $ErFe_{12-x}Nb_x$ at 4.2 K and room temperature (RT). The errors for the data in each column were derived from the data fits and are as given for each first entry.

x	T (K)	B_{hf} (T)			$\langle B_{hf}\rangle$ (T)	μ_{Fe} (μ_B)
		8i	8j	8f		
0.6	4.2	34.2(2)	30.9(2)	26.3(2)	30.3	1.9_4
	RT	28.8	26.0	22.1	25.4	1.6_3
0.7	4.2	34.1	30.7	26.1	30.1	1.9_3
	RT	28.7	25.8	22.0	25.3	1.6_2
0.8	4.2	33.8	30.5	25.9	29.8	1.9_1
	RT	28.4	25.6	21.8	25.0	1.6_1

by two sextets with fractional areas of 0.132 and 0.166, and the 8f and 8j sextets by two sextets of fractional areas 0.183 and 0.168 (these pairs of sextets represent iron atoms without near-neighbour Nb atoms and with near-neighbour Nb atoms), with similar fractional area values being calculated for the other two samples. Lorentzian lineshapes (with the same line-width for each subspectral component) were used in the fitting procedure. Emphasis was placed on fitting the 4.2 K spectrum with the final parameters being used as the basis for the initial parameters in the analysis of the higher-temperature spectra. Examples of the resultant fits are shown in figure 5 for the $ErFe_{11.4}Nb_{0.6}$ compound with the individual subspectra shown for the 4.2 K spectrum. The assignments of the subspectra were performed by taking into account the nearest-neighbour environment of each respective site and the Fe–Fe distances. The largest B_{hf} is assigned to the 8i site which has the largest Fe coordination, i.e. 5(8i), 4(8j), 4(8f). Even though the 8j and 8f sites have the same Fe coordination and 8f has the shortest mean Fe–Fe nearest neighbour distance (∼2.5 Å) as discussed previously [24, 25], the lowest B_{hf} is attributed to the 8f site. The corresponding hyperfine parameters are listed in table 2. Assuming a conversion coefficient of 15.6 T/μ_B [2], the three subspectral components for $ErFe_{11.4}Nb_{0.6}$ at 4.2 K (with average hyperfine fields of B_{hf} ∼ 34.2, ∼30.9 and ∼26.3 T) correspond to Fe moments of 2.2, 2.0 and 1.7 μ_B, for the 8i, 8j and 8f sites, respectively. This hierarchy is also observed in other $RFe_{12-x}M_x$ compounds (M = Ti, Mo, Ta, W [10, 26, 11, 12], respectively; see also [1]), although such behaviour is not the only trend noted in the literature [1]. This leads to an average Fe moment of 1.94 μ_B for $ErFe_{11.4}Nb_{0.6}$ at 4.2 K.

The temperature dependences of the hyperfine parameters for $ErFe_{12-x}Nb_x$ are illustrated by the results for $ErFe_{11.4}Nb_{0.6}$ shown in figure 6. The temperature dependence of the average hyperfine field is well fitted by the equation

$$B_{hf}(T) = B_{hf}(0)\left\{1 - b\left(\frac{T}{T_C}\right)^2\right\}. \tag{3}$$

The value of the hyperfine field at 4.2 K has been taken as $B_{hf}(0)$ and the fitted value of the constant b is 0.46(2). It has been reported that in R_2Fe_{17}-based compounds the temperature dependence of hyperfine fields also follows the above equation with a constant $b = 0.5$ for R_2Fe_{17} (R = Y, Nd, and Dy) [20, 27] and 0.53 for $HoErFe_{15}Ga_2$ [28]. The T^2 dependence of the hyperfine fields in the present series of compounds suggests that single-particle excitations may be responsible for suppressing the 3d sublattice magnetization with increasing temperature [27, 28].

The correlation between the ^{57}Fe isomer shift δ and the Wigner–Seitz cell (WSC) volume available to the iron atoms in R_2Fe_{17} and $RFe_{11}Ti$ and their interstitial compounds has proved to be very successful in delineating the electronic structure of these compounds [24, 25].

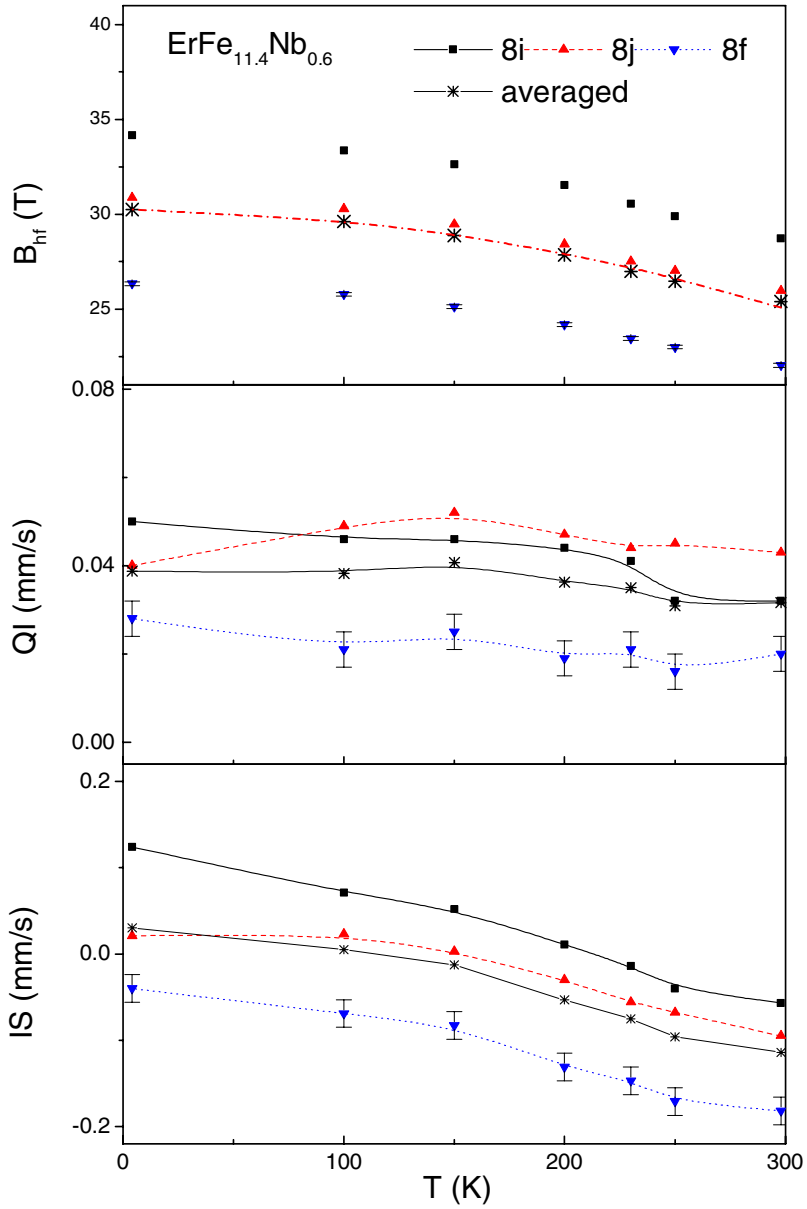

Figure 6. Temperature dependence of the ^{57}Fe hyperfine interaction parameters of $ErFe_{11.4}Nb_{0.6}$ (IS isomer shift; QI quadrupole interaction; B_{hf} magnetic hyperfine field). The values for the individual 8i, 8j and 8f sites are shown, along with the average value. For clarity, the error bars are shown only for the 8f site. The dashed line through the average magnetic hyperfine values is a fitted curve of average hyperfine fields to $B_{hf}(T) = B_{hf}(0)[1 - b(T/T)^2]$ as discussed in the text.

We have therefore calculated the WSC volumes with the BLOKJE program [29] for all the crystallographic sites in $ErFe_{12-x}Nb_x$ by using the structural and positional parameters and the twelve-coordinated metallic radii of 1.78, 1.26 and 1.46 Å for Er, Fe and Nb, respectively. As an example, the calculated WSC volumes for the 2a, 8i, 8j and 8f sites in $ErFe_{11.4}Nb_{0.6}$

are 29.3, 12.7, 11.8 and 11.3 Å^3, respectively, with the same sequence occurring in the other two compounds. It can be seen from figure 6 that the relation $\delta_{8i} > \delta_{8j} > \delta_{8f}$ is obeyed at all temperatures; this agrees with the relationship between the isomer shift and the WSC volumes (the larger the WSC volume, the larger the isomer shift δ). Moreover, the 8i, 8j and 8f sites and the site-averaged isomer shift increase with decreasing temperatures.

4. Conclusions

Our investigation of the magnetic properties of $ErFe_{12-x}Nb_x$ compounds ($x = 0.6$, 0.7, 0.8) indicates that Nb atoms preferentially occupy the 8i sites, consistent with the behaviour observed in other $R(Fe, M)_{12}$ systems (e.g. M = Ti, Ta and W [10–12]). The spin reorientation temperatures in $ErFe_{12-x}Nb_x$ remain essentially unchanged ($T_{sr} \sim 42$–44 K) with increasing Nb concentration. The sixth-order term $B_{60}O_{60}$ of the crystal field acting on Er^{3+} plays a critical role in determining the overall behaviour of the spin reorientation. The observed T^2 dependence of the ^{57}Fe hyperfine field indicates that the Fe sublattice magnetization is associated with a single-particle excitation mechanism. The average moment values at 4.2 K show a slight decrease with increasing Nb content (1.9_4 μ_B, 1.9_3 μ_B and 1.9_1 μ_B for $x = 0.6$, 0.7 and 0.8, respectively) with magnetic moments in the individual sites behaving as $\mu_{8i} > \mu_{8j} > \mu_{8f}$ (e.g. 2.2 μ_B, 2.0 μ_B and 1.7 μ_B for the 8i, 8j and 8f sites in $ErFe_{11.4}Nb_{0.6}$, respectively) as also observed in related $R(Fe, M)_{12}$ systems (e.g. [1, 10–12, 26]).

Acknowledgments

This work is supported in part by a Discovery Grant from the Australian Research Council leading to the award of a Research Associateship to JLW.

References

[1] Li H-S and Coey J M D 1991 *Handbook of Magnetic Materials* vol 6, ed K H J Buschow (Amsterdam: North-Holland) p 1
[2] Hu B, Li H S, Gavigan J P and Coey J M D 1989 *J. Phys.: Condens. Matter* **1** 755
[3] Vndreev A, Kudrevatykh N V, Razgonyaev S M and Tarasov E N 1993 *Physica* B **183** 379
[4] Kuz'min M D 2000 *J. Appl. Phys.* **88** 7217
[5] Wang J L, Fuquan B, Tang N, Yang D, Shen Y P, Yang C P, Yang F M and de Boer F R 1999 *J. Alloys Compounds* **289** 228
[6] Wang J L, Garcia-Landa B, Marquina C, Ibarra M R, Yang F M and Wu G H 2003 *Phys. Rev.* B **67** 14417
[7] Wang J L, Tang N, Shen Y P, Yang D, Fuquan B, Wu G H, Yang F M, de Boer F R, Brück E and Buschow K H J 2002 *J. Appl. Phys.* **91** 2165
Fuquan B, Wang J L, Tegus O, Dagula W, Tang N, Yang F M, Wu G H, Brück E, de Boer F R and Buschow K H J 2005 *J. Magn. Magn. Mater.* **290/291** 1192
[8] Juan R-C 1990 *The 15th Congr. Int. Union of Crystallography, Proc. Satellite Mtg On Powder Diffraction (Toulouse, France)* p 127 (http://www-llb.cea.fr/fullweb/)
[9] de Boer F R, Boom R, Mattens W C M, Miedema A R and Niessen A K 1988 *Cohesion in Metals (Transition Metal Alloys)* vol 1, ed F R de Boer and D G Pettifor (Amsterdam: North-Holland) p 1
[10] Piquer C, Hermann R P, Grandjean F, Isnard O and Long G J 2003 *J. Phys.: Condens. Matter* **15** 7395
[11] Piquer C, Palacios E, Artigas M, Bartolomé J, Rubín J, Campo J and Hofmann M 2000 *J. Phys.: Condens. Matter* **12** 2265
[12] Plugaru N, Rubín J, Bartolomé J, Piquer C and Artigas M 2002 *Phys. Rev.* B **65** 134419
[13] Stefanski P and Ivanov V 1995 *J. Alloys Compounds* **219** 199
[14] Pareti L, Solzi M, Marusi G, Ibarra M and Algarabel P A 1992 *J. Appl. Phys.* **70** 3753
[15] Algarabel P A, Pareti L, Marquina C, Solzi M, Ibarra M R and Marusi G 1992 *J. Appl. Phys.* **71** 366
[16] Garcia-Landa B, Fruchart D, Gignoux D, Soubeyroux J L and Vert R 1998 *J. Magn. Magn. Mater.* **182** 207

[17] Yang C P, Wang Y Z, Hu B P, Wang J L, Wang Z X, Jiang Z L, Ma C L and Zhu J 1999 *J. Alloys Compounds* **290** 144
[18] Cadogan J M, Ryan D H, Moze O, Swainson I P and Suzuki K 2003 *J. Appl. Phys.* **93** 6972
[19] Christides C, Anagnostou M, Li H S, Kostikas A and Niarchos D 1991 *Phys. Rev.* B **44** 2182
[20] Franse J J M and Radwanski R J 1993 *Handbook of Magnetic Materials* vol 7, ed K H J Buschow (Amsterdam: North-Holland) p 307
[21] Abadia C, Algarabel P A, Garcia-Landa B, Ibarra M R, del Moral A, Kudrevatykh N V and Markin P E 1998 *J. Phys.: Condens. Matter* **10** 349
[22] Hu B P, Li H S, Coey J M D and Gavigan J P 1990 *Phys. Rev.* B **41** 2221
[23] Wang J L, Cadogan J M and Campbell S J 2005 in preparation
[24] Hautot D, Long G J, Grandjean F and Isnard O 2000 *Phys. Rev.* B **62** 11731
[25] Long G J, Hautot D, Grandjean F, Isnard O and Miraglia S 1999 *J. Magn. Magn. Mater.* **202** 100
[26] Hien V T, Le Breton J M, Hien N T, Tai L T, Thuy N P, Duc N H, Duong N P and Teillet J 2001 *J. Magn. Magn. Mater.* **237** 10
[27] Gubbens P C M and Buschow K H J 1982 *J. Phys. F: Met. Phys.* **12** 2715
[28] Venkatesan M, Varadaraju U V and Rama Rao K V S 2001 *Phys. Rev.* B **64** 94427
[29] Gelato L 1981 *J. Appl. Crystallogr.* **14** 151